Quantifying the impact of bedrock topography uncertainty on 100-year Pine Island Glacier projections

Andreas Wernecke[1,2,3], Tamsin L. Edwards[4], Philip B. Holden[1], Neil R. Edwards[1], Stephen L. Cornford [5]

[1]The Open University, Milton Keynes, UK
[2]Max-Planck-Institute for Meteorology, Hamburg, Germany
[3]Universität Hamburg, Hamburg, Germany
[4]Kings Collage London, London, UK
[5]Faculty of Science and Engineering, Swansea University, Swansea, UK

Key Points:

- Uncertainty in topography estimates has a significant impact on predictions
- BedMachine topography simulations within range of uncertainty, Bedmap2 more stabilizing
- Pine Island Glacier is predicted to transition into more unstable state late mid-century for strong climate forcing

Corresponding author: Andreas Wernecke, andreas.wernecke@mpimet.mpg.de

Abstract

The predicted Antarctic contribution to global-mean sea-level rise is one of the most uncertain among all major sources. Partly this is because of instability mechanisms of the ice flow over deep basins. Errors in bedrock topography can substantially impact the resilience of glaciers against such instabilities. Here we analyze the Pine Island Glacier topography to derive a statistical model representation. Our model allows for inhomogeneous and statistically dependent uncertainties and avoids unnecessary smoothing from spatial averaging or middle-of-the-road interpolation. A set of topographic fields is generated which properly represents the topographic uncertainty in our ice sheet model simulations with lower and upper end climate forcings. The bedrock uncertainty alone creates a 5% to 25% uncertainty in the predicted 100-year sea level rise contributions. Ice sheet model simulations on this new set are consistent with simulations on the frequently used BedMachine topography but diverge from Bedmap2 simulations.

Plain Language Summary

We investigate the impact of uncertainties in the elevation of the bedrock underneath the ice of a particularly vulnerable glacier in Antarctica. Our approach allows us for the first time to estimate how much future projections depend on knowledge of the bedrock elevation. A main focus of this study is to represent our current expertise of the bedrock elevation as closely as possible so that our simulations accurately reflect the extent of our knowledge of the future glacier behaviour. In summary, we find that the mass of ice lost in 100-year simulations, which contributes to the global mean sea level, can be affected by up to 25%. This highlights the value of closely-spaced bedrock measurement and of careful consideration of related uncertainties in ice-sheet simulations.

1 Introduction

The Antarctic ice sheet is one of the major sources of global sea level rise and is currently losing mass at a rate of around 0.5 to 0.6 mm global mean Sea Level Equivalent per year (mm SLE a^{-1}), predominantly in the Amundsen Sea Embayment (ASE) area of the West Antarctic Ice Sheet (WAIS) (Shepherd et al., 2018; Bamber et al., 2018). The future response of the Antarctic ice sheet to a changing climate is one of the least well understood aspects of climate predictions (Oppenheimer et al., 2019).

Changes in the Antarctic ice sheet mass balance are largely governed by changes in the Surface Mass Balance (SMB) and ocean forcing via dynamical processes such as changing buttressing from ice shelves. Ice shelves, the floating extensions of grounded ice streams, can be weakened by elevated ocean and/or atmospheric temperatures and consequently melt or collapse. Buttressing ice shelves have a stabilising effect on the ice sheet with the potential to suppress or delay Marine Ice Sheet Instability (MISI) (Schoof, 2007; Joughin & Alley, 2011). MISI can occur at ice sheets on retrograde (upsloping in flow direction) topographies below sea level. Here a retreat of the grounding line (the transition from grounded to floating ice) will increase the ice thickness above it. For idealised conditions the mass flux across the grounding line increases rapidly with the ice thickness (Schoof, 2007). This additional mass loss can lead to an imbalance of the system causing a further retreat of the grounding line. Large areas of the WAIS, including Pine Island Glacier (PIG), one of the two major glacial systems of the ASE, lie on such retrograde slopes (Fretwell et al., 2013).

In the satellite record the ASE shows significant rates of thinning (Rignot et al., 2008; Mouginot et al., 2014; Shepherd et al., 2018), which have been linked to enhanced ocean melt from warm Circumpolar Deep Water entering the continental

shelf (Dutrieux et al., 2014; Naughten et al., 2018; Rignot et al., 2014). This might have triggered Marine Ice Sheet Instability in the ASE at present (Joughin et al., 2014; Favier et al., 2014; Alley et al., 2015). Bamber and Dawson (2020) find a recent reduction of rates of mass loss from PIG even though it has maintained a negative mass balance and elevated flow speeds. This behaviour could be related to lower ocean temperatures in 2012-2013 compared with the 2000s (Milillo et al., 2017). In summary, PIG currently loses mass, shows strong sensitivity to ocean-induced melt and is situated on a bedrock topography which makes it more vulnerable.

Predictions of the dynamic ice sheet response are challenging because of poorly observed local physical properties of the ice and the bedrock underneath. One of these factors concerns the bedrock elevation maps which suffer from errors from the instruments and gaps in the record. The lack of local measurements creates a need for spatial interpolation which adds additional uncertainties. It is worth highlighting that MISI depends on the topography gradient local to the grounding line. Topography measurement errors and interpolation are likely to have a stronger relative impact on gradients than on the absolute elevation.

Here we generate statistically a set of bedrock topographies which represent the range of uncertainties from topographic observations and interpolation. These topographies are therefore in agreement with observational constraints while aiming to fully represent their uncertainties. We then assess the impact of topographic uncertainties by using the set of bedrock topographies in an ensemble of ice sheet model simulations. We use the BISICLES ice sheet model to simulate PIG changes this century under two climate forcings – low, and strongly increasing - using three different friction laws. Thereby we show how bedrock uncertainty translates into predictive uncertainty for a large range of plausible future scenarios, friction laws and topographies.

In Section 2 we will introduce the airborne radar measurements used here and analyse the geostatistical properties. Based on this we set up simulations of the ice sheet model BISICLES in Section 3, starting with the generation of topographies, initialisation and inversion of model parameters, followed by a description of the forcing we use for 100-year simulations. Simulation results are presented in Section 4 with focus on the contribution to uncertainty in sea level, and are discussed in Section 5.

2 Data and Methods

We summarize our knowledge of the real bedrock in a multivariate random variable which is approximated by a Gaussian Process (GP). By using this statistical model, we can represent uncertainties in elevation observations considered as random variables, by sampling spatial fields of bedrock topography within the range of local uncertainties and spatial covariance structure. To define a GP model we need training data and covariance function parameters. Ungridded airborne radar measurements are analysed to estimate the statistical characteristics of the bedrock topography and measurement uncertainties. This provides us with the required GP model covariance function parameters. We train the GP to match observed values, given the observational uncertainty. From this GP model we draw random samples to represent the topography and its uncertainty in the ice sheet model BISICLES.

The airborne Radar Echo Sounding (RES) dataset used here is compiled from two different sources, namely the one described in Holt et al. (2006), and Operation Ice Bridge IRMCR2 Level-2 data from October 2009 to December 2017 (Paden et al., 2010, NSIDC, last accessed in September 2019 through https://cmr.earthdata.nasa.gov). These radar measurements do not measure bedrock topography underneath ice shelves. The PIG catchment area is defined as in Mouginot et al. (2017) based on Rignot et al. (2013). About 1.5% of the 2.3 million measurements in this basin are removed here due

to inconsistencies. For training, the RES dataset has to be sub-sampled to reduce its size, due to computational constraints. This is done by imposing a 2 km × 2 km grid onto the region and randomly selecting one measurement from each box if available (about 25 000 measurements). This is done to ensure a good spatial coverage while avoiding smoothing effects from averaging. The covariance function is derived from semivariograms on fully random (no use of boxes) subsets of 100 000 measurements. Exponential functions are fitted to the semi-variance on scales of 25 km to 50 km to derive the nugget, length scale and far-field variance to describe the spatial correlation characteristics. These exponential fits capture the semivariance very well (Wernecke, 2020, section 5.1.2) which motivates our use of an exponential covariance function for the GP.

The exponential covariance function, c_E, is defined as:

$$COV(x_1, x_2) = c_E(r, \sigma_c^2, \ell) = \sigma_c^2 \exp\Big(-\frac{r}{2\ell}\Big), \tag{1}$$

where $COV(x_1.x_2)$ is the covariance in the bedrock topography at the locations x_1 and x_2, σ_c^2 is the far-field variance (or sill), r is the physical distance between the locations x_1 and x_2 and ℓ is the characteristic correlation length scale. The randomized sub-sampling for deriving the covariance parameters and the training data is repeated to capture the impact on the final simulations. See Wernecke (2020) Section 5.1.2 for more information.

We generate random two-dimensional sample fields within the range of the local measurement uncertainties which also adhere to the full spatial covariance matrix and with it the uncertainty estimate, as illustrated in Figure 1a. The topographic uncertainty is clearly increasing with distance to the closest measurement (flight line) and is often above 50 m (one standard deviation), even in regions with close sampling.

The computational demand of sampling from a GP scales with the number of spawned grid cells n by $\mathcal{O}(n^3)$, which imposes a limit on this number. We use the python GPy module to draw 12 samples on a 4 km×4 km grid in the PIG catchment area. We use Bedmap2 geometry (bedrock topography and ice thickness), brought to the same resolution by averaging, for the remainder of the rectangular model domain and ungrounded area. The ice surface elevation is considered well known and the ice thickness is adjusted for all statistically generated topographies to match the Bedmap2 surface elevations. The resulting 12 topographies are accompanied by two reference topographies, Bedmap2 (Fretwell et al., 2013) and BedMachine (Morlighem, 2019; Morlighem et al., 2020), with the same resolution.

3 Simulations

We use all combinations of the 14 topographies described above with three friction laws and two climate forcings, resulting in a total of 84 simulations. The simulations are performed by the adaptive mesh ice sheet model BISICLES (Cornford et al., 2013, 2015), which is a finite-volume model with vertically integrated stress approximations (Wernecke, 2020, sections 2.1 and 5.2.2 for more information). Each topography is used separately to find basal traction coefficient and effective viscosity fields for PIG using the BISICLES inverse model framework with a compilation of satellite based ice surface velocities from Rignot et al. (2017, 2011). Figure 1b illustrates the initial velocity field of the main PIG trunk.

The Weertman friction law is :

$$\tau_b = C_m \cdot |u_b|^{m-1} \cdot u_b$$

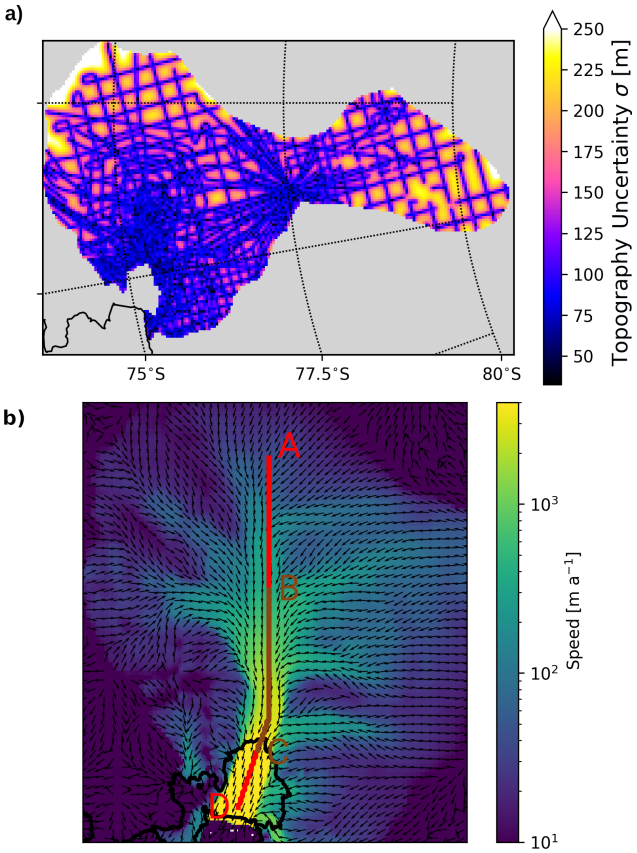

Figure 1. a: One standard deviation of trained GP which increases with distance from measurements (flight lines) and b: Initial PIG ice velocity direction (arrows) and speed (colours), for the main trunk (left half of panel a) of PIG flow including the approximate central flow line (red and brown).

with τ_b being the basal stress tangential to the base of the ice, C_m is the spatially varying basal traction coefficient for a given friction law exponent m and u_b is the basal ice velocity. We use $m = 1$ for linear friction, $m = 1/3$ for nonlinear friction and $m = 1/8$ for strongly nonlinear friction (called plastic friction in the following). Ice flow outside of the PIG catchment area is suppressed for numerical stability.

3.1 Climate forcing

For the model simulations we use two different climate forcings with changing ocean melt and SMB. These two forcings are intended to encompass the range of likely climate scenarios:

- The **low forcing** uses an RCP2.6 SMB and constant-in-time ocean melt rates.
- The **high forcing** uses an RCP8.5 SMB and linearly increasing ocean melt, starting at the low forcing rates at the beginning and adding 200 % by the end of the 100-year model simulations

As SMB we use data from NorESM1-M, a CMIP5 atmosphere-ocean coupled global climate model (Bentsen et al., 2013). Of the three models selected in Barthel et al. (2020) for the ice sheet model intercomparison project ISMIP6 (Seroussi et al., 2020) for consistency with the CMIP5 multi-model ensemble, NorESM1-M has the highest rank in the CMIP5 cross-model performance analysis by Agosta et al. (2015). The simulations show below median atmospheric warming and relatively strong 21st century ocean warming compared with the multi-model ensemble (Barthel et al., 2020).

The ocean melt at the beginning of the simulations is based on temperature and salinity profiles corresponding to the Warm_0 setup in Favier et al. (2019) which is based on oceanographic measurements from Dutrieux et al. (2014). The profiles have warm and salty water at depth and colder, fresher water towards the surface. This structure is caused by the overturning circulation of warm Circumpolar Deep Water which mixes with glacial meltwater before being transported offshore near the surface. We use a local squared ocean melt forcing parameterisation since it is the best local parameterisation in Favier et al. (2019). The resulting total PIG initial melt rate of 84.6 Gt a^{-1} (using Bedmap2 geometry) is in good agreement with other estimates (Jourdain et al., 2020; Dutrieux et al., 2014; Rignot et al., 2013).

Predictions of future ocean melt forcing are highly uncertain, but cannot be ignored for 100-year model simulations. The two forcings used here are designed to represent reasonable low and high melt scenarios without being bound to specific climate projections. Naughten et al. (2018) use the Southern Ocean quality of 19 CMIP5 models to select a forcings for the regional ocean model FESOM. The ocean model predicts a year 2100 ASE ocean melt increase of about 200% (multi-model mean) to 300% (ACCESS-1.0) for RCP8.5. However, Naughten et al. (2018) note a cold bias of about 2 K in the bottom water temperature on the Amundsen Sea continental shelf at the beginning of the simulations. They argue that the warming should be seen largely as reversal of a model bias which makes it very likely that the increase in melt is overestimated. This overestimation might be up to about 150% in melt increase (Wernecke, 2020, Section 5.2.3). We select an increase of 200% in 100 years as a best guess upper-end melt representation.

We cannot rule out that current ocean conditions are a positive anomaly caused by internal variability. Climate projections of ice shelf ocean melt rates for the ASE often show positive trends (Naughten et al., 2018; Alevropoulos-Borrill et al., 2020; Jourdain et al., 2020), but some projections show temporarily negative ocean temperature anomalies compared to the early 2000s (Jourdain et al., 2020; Alevropoulos-Borrill

et al., 2020). We apply a constant ocean melt forcing, consistent with recent past rates, as reasonable lower-end forcing.

4 Results

4.1 Simulations

In the first years we see high-amplitude small spatial-scale rates of ice thickness change which diminish over time (Wernecke, 2020, Section 5.3.2). This is an adjustment of the model to a self-consistent state. In retrospect we should have implemented a spin-up period in the simulations with a constant forcing before the forced projections start. Instead our simulations start with forcing, including SMB corresponding to year 2000 AD (used as start year). By careful inspection (Wernecke, 2020, Section 5.3.2) we define the 15th year as reference which is used as baseline for the following calculations. In this way the impact of initial adjustments on the results is minimized.

While the statistically generated topographies agree well with the reference topographies (in particular BedMachine) on average, the samples used for simulations (e.g. Figure 2, right) show stronger regional variability. The scale of this variability is in agreement with very high-resolution observations (Bingham et al., 2017; Wernecke, 2020, Section 5.3.1). For GP samples topography uncertainties are represented within the sample while Bedmap2 and BedMachine use averaging and interpolation techniques which create smoother fields (with spatially localised uncertainties).

The ice geometry and flow speed along the downstream sector of the central PIG flow line (from location B to D in Figure 1b) is illustrated for plastic friction and Bedmap2 as well as BedMachine in Figure 2, left. For low forcing the glacier thins slightly without the grounding line retreating much. At the same time the ice speed reduces, in particular in the fast-flowing ice shelf. Note that PIG is currently out-of-balance so that a (stabilizing) slow-down is not contradicting further mass loss. A partial slow-down of the PIG ice velocities is also predicted for the flow line model simulations in Gladstone et al. (2012) and is found in the optimized (central) simulations from Nias et al. (2016) for all combinations of bedrock and friction law (not shown).

For the high forcing scenario we see very different pictures for BedMachine and Bedmap2 geometries: For BedMachine the ice near the grounding line accelerates over the 85 year projection period from less than 4000 m a^{-1} to more than 5000 m a^{-1}. The speed-up extends more than 150 km upstream (red lines in Figure 2). For Bedmap2 the high forcing scenario does not show noteworthy acceleration or thinning.

The flow line characteristics of two topographies generated here are shown on the right of Figure 2. Simulations with statistically generated topographies share the same features of those using BedMachine: little changes to the ice geometry with some slow-down for low forcing, and pronounced thinning with significant grounding line retreat and accelerating ice for high forcing.

4.2 Sea level rise contribution

The ensemble behaviour can be categorized into two states, a steadily evolving state with approximately constant rates of mass loss (about 0.1 mm SLE a^{-1}) and an unstable state with mass losses up to six times faster (Figure 3, top). The timing of an ensemble member to become unstable depends strongly on the topography and forcing: most high melt simulation become unstable between 2055 and 2075. This timing seems not to depend on the friction law (Figure 3, top right). Low melt ensemble members remain in the steadily evolving state without exception.

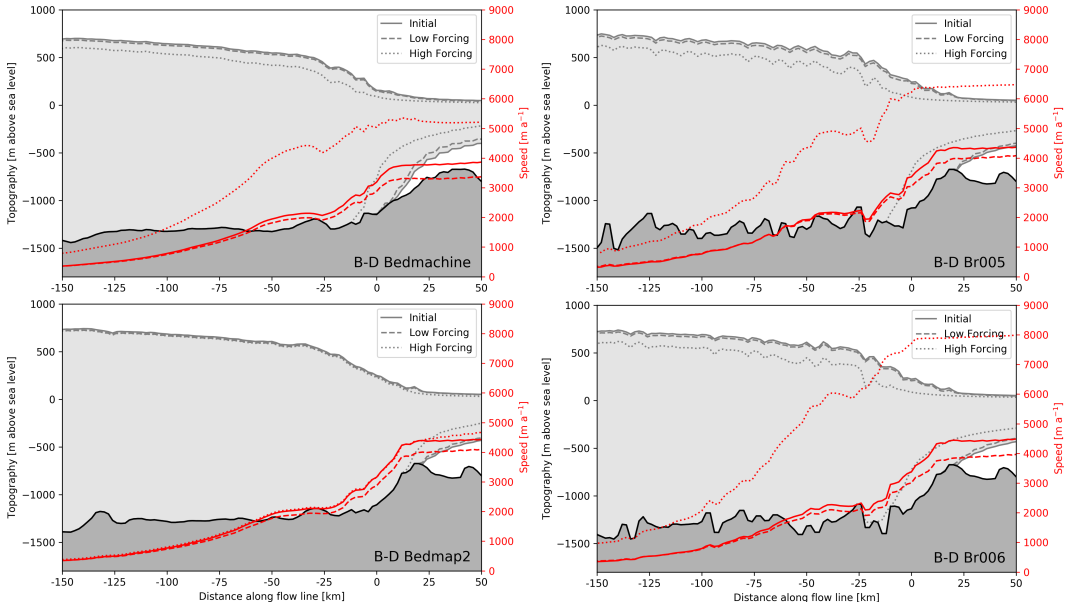

Figure 2. Profiles along PIG flow line from location B to D in Figure 1 with BedMachine (top left) and Bedmap2 (bottom left) and two statistically generated topographies (right). Shown are the bedrock underneath the ice (black), surface and basal ice boundaries (grey) and the ice speed (red) after 15 years of simulation (used as baseline; solid lines) and at the end of the 100-year simulations with high (dotted) and low (dashed) forcing, all using a plastic friction law.

Table 1. Mean 2100 sea level contribution estimates (relative to 2015) with one standard deviation of the statistically generated bedrock ensemble (both in mm SLE)

Friction law:	Linear	Nonlinear	Plastic
High Forcing:	11.3 ±2.08	15.5 ±3.86	19.4 ±5.15
Low Forcing:	6.7 ±0.31	5.6 ±0.62	4.7 ±0.87

The main effect of the friction law is an increase in the rate of mass loss in the unstable state with faster rates for more non-linear friction laws (Figure 3, middle). For low forcing the relationship is reversed, more linear friction leads to larger sea level contributions. This can be traced back to the slow down of the ice velocities as shown in Figure 2. Highly nonlinear friction laws facilitate decelerating ice to slow down even more and accelerating ice to speed up more than linear counterparts. This also explains why the predictive uncertainty due to the bedrock uncertainty strongly increases with non-linearity of the friction law and with stronger forcing. The standard deviation of the net sea level contribution over the 85-years ranges from 0.31 mm SLE for low forcing and linear friction to 5.15 mm SLE for high forcing and plastic friction which corresponds to about 5% to 25% of total sea level contribution (Figure 3 middle and Table 1).

BedMachine based simulations agree with simulations based on topographies generated here regarding the total sea level contribution. In contrast, Bedmap2 runs with high forcing are not consistent with the behaviour for all other topographies used. Instead Bedmap2 sea level rise contributions remain in the more stable, steadily evolving state regardless of forcing (Figure 3 bottom). This suggests that Bedmap2 has an overly stabilising effect on PIG, even for strong melt forcing and plastic friction.

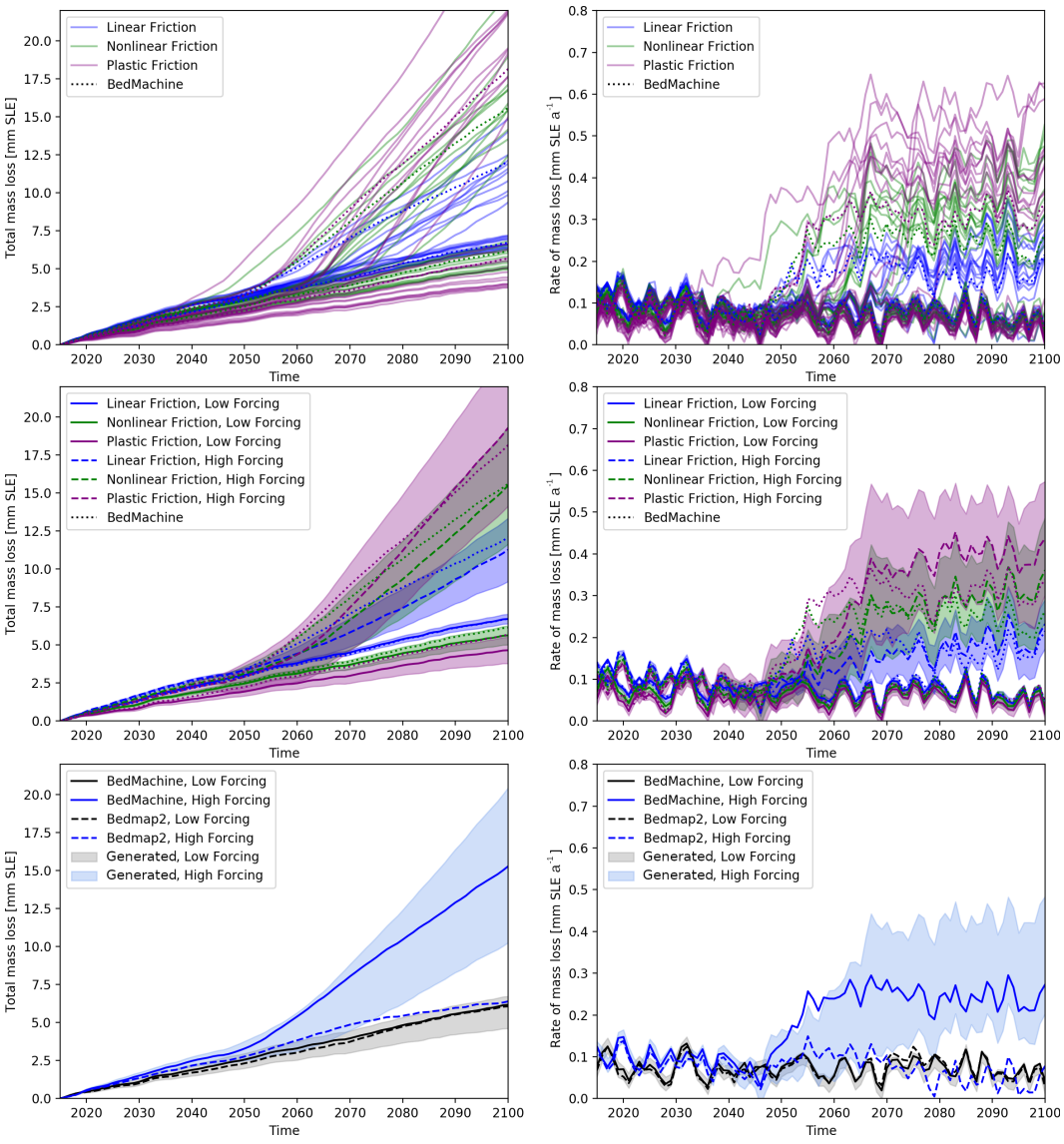

Figure 3. Net sea level contribution (left) and yearly rate (right). Individual simulations (top), grouped by friction law and forcing (middle) and grouped only by forcing including Bedmap2 (bottom). Shades correspond to ± one standard deviation.

5 Discussion

Present-day bedrock topography uncertainty has been shown to have a strong influence on ice sheet simulations in the mid-Pliocene where the sea level contribution in 3000-year simulations varies between 12.6 and 17.9 m SLE for different noise realisations (Gasson et al., 2015). The sensitivity of BISICLES to roughness in the topography has been investigated by Sun et al. (2014) by adding noise of different spatial scales to a reference topography. The strongest impact is found for the largest scale (50 km) which, just as for our high forcing scenario, determines the timing of the system to transition into a more unstable state. In contrast to such sensitivity studies, our sample is representative of our knowledge about the topography, including likely correlation length scales and an increase in topography uncertainty with distance to measurements.

Simulations based on Bedmap2 for PIG show less sensitivity to strong climate forcing than the statistically generated topographies and BedMachine. Since our topographies agree qualitatively with BedMachine it is unclear what aspect causes the difference: BedMachine uses a mass conservation approach where topographies are relaxed to avoid large mass flux divergence (positive or negative) from unreasonable ice geometry-velocity combinations. Our topographies and Bedmap2 do not include such considerations but share a sill near the grounding line. Our topographies show at the same time considerably more variability than the relatively smooth Bedmap2 and BedMachine. We do note, however, that the Bedmap2 topography lies largely above the others within the first approximately 150 km upstream from the grounding line and that, for the same surface elevation of the ice, an elevated topography is further from hydrostatic equilibrium and could hence be less prone to retreat. Whatever the reason, the striking underestimation of mass loss for Bedmap2 simulations and high forcing relative to the other topographies (Figure 3, bottom), calls for caution in interpreting modelling results obtained with this topography.

The simulations used here have no representation of Marine Ice Cliff Instability which cannot be ruled out on these timescales. It seems, however, not possible at the moment to represent it in a well constrained way, or to predict how strong its impact could be on simulations up to year 2100.

Another clear limitation of our simulations is the resolution of statistically generated topographies of 4 km $\times$ 4 km (which is interpolated up to 500 m within the adaptive grid refinement of BISICLES). The reason for this is not so much the Gaussian Process approach itself but the relatively high computational demand of a Cholesky decomposition which is used to generate random samples from a large covariance matrix. Evaluations of the mean field ('best estimate') would have been possible on fine resolutions, but would not have covered all of the uncertainties. It is challenging to quantify the impact of the bedrock resolution, but it should be noted that the statistically generated topographies contain much more variability than both reference topographies, and that finer resolutions would, if anything, amplify this property. Simulations using Bedmap2 topography at 1 km resolution behave very similarly to those with degraded 4 km resolution (not shown).

To represent bedrock uncertainty in future simulations it would be desirable to have reference realizations, like the set of topographies we generated here but for more general setups (ideally continent wide). This would allow different modelling groups to represent topographic uncertainty in predictions while retaining comparability (since the same samples are used). Similar approaches could be used to assess the value of additional measurements, e.g. for planning future campaigns.

In conclusion, we have been able to couple the representation of the bedrock uncertainty more closely to observational constraints in combination with the use of

realistic climate forcings. In particular we have shown how the uncertainty from topography interacts with other model parameters. This uncertainty increases with nonlinearity of the friction law and with stronger (melt) forcing. One standard deviation can make up between 5% and about 25% (=5 mm SLE) of the 85-year signal, solely due to uncertainties in topography measurements and interpolation. These predictive uncertainties have been known to exist but until now remained largely omitted and unquantified. The low forcing scenario, which is more likely to be realized in very low greenhouse gas emission scenarios, would limit the PIG contribution to global mean sea level in this century. In addition we find the use of Bedmap2 to be likely to lead to an underestimation of the dynamic response of PIG and recommend the use of BedMachine if a reference topography has to be used.

6 Open Research

The simulations and bedrock topographies are publicly accessible at https://doi.org/10.5281/zenodo.5553288, https://doi.org/10.5281/zenodo.5553311 and https://doi.org/10.5281/zenodo.5553320 (linear, nonlinear and plastic friction, respectively).

Acknowledgments

We would like to thank Jonty Rougier for inspirational discussions on this project. AW was supported by The Open University in form of a scholarship at the time of conducting this research. We want to acknowledge the University of Bristol to provide us with computational resources from the Advanced Computing Research Centre where the BISICLES simulations were carried out.

References

Agosta, C., Fettweis, X., & Datta, R. (2015). Evaluation of the cmip5 models in the aim of regional modelling of the antarctic surface mass balance. *The Cryosphere*, *9*, 2311–2321.

Alevropoulos-Borrill, A. V., Nias, I. J., Payne, A. J., Golledge, N. R., & Bingham, R. J. (2020). Ocean-forced evolution of the amundsen sea catchment, west antarctica, by 2100. *The Cryosphere*, *14*, 1245–1258.

Alley, R. B., Anandakrishnan, S., Christianson, K., Horgan, H. J., Muto, A., Parizek, B. R., ... Walker, R. T. (2015). Oceanic forcing of ice-sheet retreat: West antarctica and more. *Annual Review of Earth and Planetary Sciences*, *43*, 207–231.

Bamber, J. L., & Dawson, G. J. (2020). Complex evolving patterns of mass loss from antarctica's largest glacier. *Nature Geoscience*, *13*(2), 127–131.

Bamber, J. L., Westaway, R. M., Marzeion, B., & Wouters, B. (2018). The land ice contribution to sea level during the satellite era. *Environmental Research Letters*, *13*(6), 063008. doi: 10.1088/1748-9326/aac2f0

Barthel, A., Agosta, C., Little, C. M., Hattermann, T., Jourdain, N. N., Goelzer, H., ... Bracegirdle, T. T. (2020). Cmip5 model selection for ismip6 ice sheet model forcing: Greenland and antarctica. *The Cryosphere*, *14*(3), 855–879.

Bentsen, M., Bethke, I., Debernard, J. B., Iversen, T., Kirkevåg, A., Seland, Ø., ... others (2013). The norwegian earth system model, noresm1-m–part 1: description and basic evaluation of the physical climate. *Geoscientific Model Development*, *6*(3), 687–720.

Bingham, R. G., Vaughan, D. G., King, E. C., Davies, D., Cornford, S. L., Smith, A. M., ... Shean, D. E. (2017). Diverse landscapes beneath pine island glacier influence ice flow. *Nature Communications*, *8*(1), 1–9. doi: 10.1038/s41467-017-01597-y

Cornford, S. L., Martin, D., Payne, A., Ng, E., Le Brocq, A., Gladstone, R., ...

Vaughan, D. G. (2015). Century-scale simulations of the response of the west antarctic ice sheet to a warming climate. *The Cryosphere*, *9*, 1579–1600. doi: 10.5194/tc-9-1579-2015

Cornford, S. L., Martin, D. F., Graves, D. T., Ranken, D. F., Le Brocq, A. M., Gladstone, R. M., ... Lipscomb, W. H. (2013). Adaptive mesh, finite volume modeling of marine ice sheets. *Journal of Computational Physics*, *232*(1), 529–549. doi: 10.1016/j.jcp.2012.08.037

Dutrieux, P., De Rydt, J., Jenkins, A., Holland, P. R., Ha, H. K., Lee, S. H., ... Schröder, M. (2014). Strong sensitivity of pine island ice-shelf melting to climatic variability. *Science*, *343*(6167), 174–178.

Favier, L., Durand, G., Cornford, S. L., Gudmundsson, G. H., Gagliardini, O., Gillet-Chaulet, F., ... Le Brocq, A. M. (2014). Retreat of pine island glacier controlled by marine ice-sheet instability. *Nature Climate Change*, *4*(2), 117–121. doi: 10.1038/nclimate2094

Favier, L., Jourdain, N. C., Jenkins, A., Merino, N., Durand, G., Gagliardini, O., ... Mathiot, P. (2019). Assessment of sub-shelf melting parameterisations using the ocean–ice-sheet coupled model nemo (v3. 6)–elmer/ice (v8. 3). *Geoscientific Model Development*, *12*(6), 2255–2283.

Fretwell, P., Pritchard, H. D., Vaughan, D. G., Bamber, J., Barrand, N., Bell, R., ... others (2013). Bedmap2: improved ice bed, surface and thickness datasets for antarctica. *The Cryosphere*, *7*, 375–393. doi: 10.5194/tc-7-375-2013

Gasson, E., DeConto, R., & Pollard, D. (2015). Antarctic bedrock topography uncertainty and ice sheet stability. *Geophysical Research Letters*, *42*(13), 5372–5377.

Gladstone, R. M., Lee, V., Rougier, J., Payne, A. J., Hellmer, H., Le Brocq, A., ... Cornford, S. L. (2012). Calibrated prediction of pine island glacier retreat during the 21st and 22nd centuries with a coupled flowline model. *Earth and Planetary Science Letters*, *333*, 191–199. doi: 10.1016/j.epsl.2012.04.022

Holt, J. W., Blankenship, D. D., Morse, D. L., Young, D. A., Peters, M. E., Kempf, S. D., ... Corr, H. F. (2006). New boundary conditions for the west antarctic ice sheet: Subglacial topography of the thwaites and smith glacier catchments. *Geophysical Research Letters*, *33*(9), L09502. doi: 10.1029/2005GL025561

Joughin, I., & Alley, R. B. (2011). Stability of the west antarctic ice sheet in a warming world. *Nature Geoscience*, *4*(8), 506–513.

Joughin, I., Smith, B. E., & Medley, B. (2014). Marine ice sheet collapse potentially under way for the thwaites glacier basin, west antarctica. *Science*, *344*(6185), 735–738. doi: 10.1126/science.1249055

Jourdain, N. C., Asay-Davis, X., Hattermann, T., Straneo, F., Seroussi, H., Little, C. M., & Nowicki, S. (2020). A protocol for calculating basal melt rates in the ismip6 antarctic ice sheet projections. *The Cryosphere*, *14*(9), 3111–3134.

Milillo, P., Rignot, E., Mouginot, J., Scheuchl, B., Morlighem, M., Li, X., & Salzer, J. T. (2017). On the short-term grounding zone dynamics of pine island glacier, west antarctica, observed with cosmo-skymed interferometric data. *Geophysical Research Letters*, *44*(20), 10–436.

Morlighem, M. (2019). Measures bedmachine antarctica, version 1. Boulder, Colorado USA. NASA National Snow and Ice Data Center Distributed Active Archive Center. (Accessed: 2020-02) doi: 10.5067/C2GFER6PTOS4

Morlighem, M., Rignot, E., Binder, T., Blankenship, D., Drews, R., Eagles, G., ... others (2020). Deep glacial troughs and stabilizing ridges unveiled beneath the margins of the antarctic ice sheet. *Nature Geoscience*, *13*(2), 132–137. doi: 10.1038/s41561-019-0510-8

Mouginot, J., Rignot, E., & Scheuchl, B. (2014). Sustained increase in ice discharge from the amundsen sea embayment, west antarctica, from 1973 to 2013. *Geophysical Research Letters*, *41*(5), 1576–1584.

Mouginot, J., Scheuchl, B., & Rignot, E. (2017). Measures antarctic boundaries for

ipy 2007-2009 from satellite radar, version 2. Boulder, Colorado USA. NASA National Snow and Ice Data Center Distributed Active Archive Center. (Accessed: 2019-07) doi: 10.5067/AXE4121732AD

Naughten, K. A., Meissner, K. J., Galton-Fenzi, B. K., England, M. H., Timmermann, R., & Hellmer, H. H. (2018). Future projections of antarctic ice shelf melting based on cmip5 scenarios. *Journal of Climate*, *31*(13), 5243–5261.

Nias, I. J., Cornford, S. L., & Payne, A. J. (2016). Contrasting the modelled sensitivity of the amundsen sea embayment ice streams. *Journal of Glaciology*, *62*(233), 552–562. doi: 10.1017/jog.2016.40

Oppenheimer, M., Glavovic, B., Hinkel, J., van de Wal, R., Magnan, A. K., Abd-Elgawad, A., ... Sebesvari, Z. (2019). Sea level rise and implications for low lying islands, coasts and communities. In *Ipcc special report on the ocean and cryosphere in a changing climate [h.-o. portner, d.c. roberts, v. masson-delmotte, p. zhai, m. tignor, e. poloczanska, k. mintenbeck, a. alegria, m. nicolai, a. okem, j. petzold, b. rama, n.m. weyer (eds.)].* The Intergovernmental Panel on Climate Change.

Paden, J., Li, J., Leuschen, C., Rodriguez-Morales, F., & Hale, R. (2010). Icebridge mcords l2 ice thickness, version 1. from oct. 2009 to dec. 2017. Boulder, Colorado USA. NASA National Snow and Ice Data Center Distributed Active Archive Center. (updated 2019, Accessed: 2019-09) doi: 10.5067/GDQ0CUCVTE2Q

Rignot, E., Bamber, J. L., Van Den Broeke, M. R., Davis, C., Li, Y., Van De Berg, W. J., & Van Meijgaard, E. (2008). Recent antarctic ice mass loss from radar interferometry and regional climate modelling. *Nature Geoscience*, *1*(2), 106–110. doi: 10.1038/ngeo102

Rignot, E., Jacobs, S., Mouginot, J., & Scheuchl, B. (2013). Ice-shelf melting around antarctica. *Science*, *341*(6143), 266–270.

Rignot, E., Mouginot, J., Morlighem, M., Seroussi, H., & Scheuchl, B. (2014). Widespread, rapid grounding line retreat of pine island, thwaites, smith, and kohler glaciers, west antarctica, from 1992 to 2011. *Geophysical Research Letters*, *41*(10), 3502–3509. doi: 10.1002/2014GL060140

Rignot, E., Mouginot, J., & Scheuchl, B. (2017). Measures insar-based antarctica ice velocity map, version 2. Boulder, Colorado USA. NASA National Snow and Ice Data Center Distributed Active Archive Center. (Accessed: 2018-11) doi: 10.5067/D7GK8F5J8M8R

Rignot, E., Velicogna, I., van den Broeke, M. R., Monaghan, A., & Lenaerts, J. T. (2011). Acceleration of the contribution of the greenland and antarctic ice sheets to sea level rise. *Geophysical Research Letters*, *38*(5), L05503. doi: 10.1029/2011GL046583

Schoof, C. (2007). Ice sheet grounding line dynamics: Steady states, stability, and hysteresis. *Journal of Geophysical Research: Earth Surface*, *112*(F3), F03S28.

Seroussi, H., Nowicki, S., Payne, A. J., Goelzer, H., Lipscomb, W. H., Abe Ouchi, A., ... Zwinger, T. (2020). Ismip6 antarctica: a multi-model ensemble of the antarctic ice sheet evolution over the 21st century. *The Cryosphere*. doi: 10.5194/tc-14-3033-2020

Shepherd, A., Ivins, E., Rignot, E., Smith, B., Van Den Broeke, M., Velicogna, I., ... Wouters, B. (2018). Mass balance of the antarctic ice sheet from 1992 to 2017. *Nature*, *558*, 219–222. doi: 10.1038/s41586-018-0179-y

Sun, S., Cornford, S., Liu, Y., & Moore, J. C. (2014). Dynamic response of antarctic ice shelves to bedrock uncertainty. *The Cryosphere*, *8*(4), 1561–1576.

Wernecke, A. (2020). *Quantifying century-scale uncertainties of the global mean sea level rise contribution from the amundsen sea sector, west antarctica* (Doctoral dissertation, The Open University). doi: 10.21954/ou.ro.0001223d